https://doi.org/10.18321/ectj1130

Genesis and Properties of MO_x/CNTs (M = Ce, Cu, Mo) Catalysts for Aerobic Oxidative Desulfurization of a Model Diesel Fuel

E.V. Matus*, S.A. Yashnik, A.V. Salnikov, L.M. Khitsova, A.N. Popova, A.P. Nikitin, S.A. Sozinov, Z.R. Ismagilov

The Federal Research Center of Coal and Coal-Chemistry of SB RAS, pr. Sovetskiy 18, Kemerovo, Russia

Article info

Received:
10 June 2021

Received in revised form:
19 August 2021

Accepted:
17 October 2021

Keywords:
Metal-carbon catalyst
Dibenzothiophene
Diesel fuel
Oxidative desulfurization

Abstract

Aerobic oxidative desulfurization of a model diesel fuel over MO_x/CNTs catalysts (M = Ce, Cu, Mo) was studied to develop innovative technology for cleaning motor fuels to EURO-5 standard. It was shown that the thermal stability of catalysts improves in the following order of metal Cu < Ce < Mo. The disordering of the carbon matrix of support increases in the next row of M: Mo < Ce < Cu, which is accompanied by an increase in the specific surface area of the samples (40 → 105 m^2/g). The forms of stabilization of the active component (CeO_2, $CuO/Cu_2O/Cu$, or MoO_3/MoO_2) were revealed, indicating a partial reduction of the metal cations during the thermal decomposition of copper and molybdenum precursor compounds deposited on CNTs. In oxidative desulfurization of a model diesel fuel over MO_x/CNTs catalysts at 150 °C the total conversion of dibenzothiophene increased in the next row of M: Ce < Cu < Mo. It was found that at 150 °C over the optimum MoO_x/CNTs catalyst the highest dibenzothiophene conversion 95–99% is observed. It was assumed that the high activity of MoO_x/CNTs is associated with both the oxidizing ability and the tendency of MoO_x to chemosorption of sulfur compounds.

1. Introduction

Sulfur dioxide is typically released during the combustion of fuels or other sulfur-containing materials. It is a pollutant that leads to acid rain, which in turn degrades soil and water quality and damages vegetation. SO_2 emissions also adversely affect human health. With population growth and an increase in fuel consumption, the sulfur content in the fuels has become a serious environmental problem, due to which research on the removal of sulfur-containing compounds is an important task. Many countries worldwide are switching to low and ultra-low sulfur fuels by updating fuel quality standards and/or modernizing refineries to produce low sulfur fuel [1]. With each new Euro standard, there is less and less sulfur in the fuel. For Euro V this is a maximum of 0.001 wt.% (10 ppmw).

All crude oil contains sulfur as an impurity – this proportion may be higher ("acidified feed", > 0.5 wt.% sulfur) or less ("sweet feed", < 0.5 wt.% sulfur). To meet the quality demands of fuel, the hydrodesulfurization (HDS) process has been commonly used by refineries [2]. HDS is a very effective technology, but the deep removal of sulfur compounds (SCs), especially heterocyclic aromatic SCs – benzothiophene (BT), dibenzothiophene (DBT), 4,6-dimethyldibenzothiophene 4,6-DMDBT), requires severe process conditions (high temperature and pressure) and high operating costs. Consequently, alternative non-HDS methods are being actively developed. In particularly, adsorptive desulfurization [3, 4], oxidative desulfurization (ODS) [5–11], oxidative-extractive desulfurization [12], photocatalytic oxidative desulfurization [13] are being studying.

Currently, researchers pay much attention to aerobic ODS, which provides the selective conversion of sulfur compounds under mild conditions and using the highly abundant oxidant – O_2 [14–19]. In aerobic ODS, one of the biggest challenges is finding a highly active catalyst. For this

*Corresponding author. E-mail: matus@catalysis.ru

process, mono- (Pt, Pd, Mn, Co, Fe, Cu, V, W), bi- (Mn-Co, Co-Mo, Ce-Mo) and multicomponent ($H_5PV_2W_{10}O_{40}$, $(NH_4)_5H_6PV_8Mo_4O_{40}$) catalytic systems supported on various types of carriers (Al_2O_3, CeO_2, SBA-15, g-BN, activated carbon) are being developed [5, 20–28]. Carbon materials occupy a special place among support and catalysts for aerobic ODS due to their structure, functional groups, or defects that can adsorb reagents, stabilize the active metal species, or be activated in relation to oxygen molecules [13, 29–33]. There are different points of view on the nature of the active centers of carbon materials in this reaction. In particular, it is established that carbonyl groups play crucial roles during the oxidation of sulfur-containing compounds over reduced graphene oxide (rGO) [13, 29]. In addition, chemically active defects also take place in this process because carbonyl groups could be generated in situ on these defects under the reaction conditions [29]. In CNTs the higher graphitization degree promotes higher catalytic activities for DBT oxidation due to higher electric conductivity, thus benefiting the transfer of electrons involved in the oxidation–reduction reaction [30].

Introducing a metal into a carbon matrix regulates its physicochemical characteristics in a wide range and can be an effective way to create composite materials with improved functional properties [34–36]. This study is a continuation of our work [37–41] on designing new nanosized catalysts for oxidative transformations of sulfur compounds of the thiophene family for developing fundamental bases of innovative principles of motor fuels upgrading to EURO-5 standard. In this work, MO_x/CNTs catalysts (M = Ce, Cu, Mo) have been prepared and comparatively studied by inductively coupled plasma optical emission spectrometry, thermal analysis coupled with mass spectrometry, low-temperature nitrogen adsorption, X-ray diffraction and structural analysis, scanning electron microscopy with EDX analysis, Raman spectroscopy and testing in oxidative desulfurization of a model diesel fuel. The regulation of the functional properties of the catalysts was achieved, and optimal composition was determined.

2. Experimental

2.1. Catalyst preparation

MO_x/CNTs(M = Ce, Mo, Cu) catalysts were prepared by the incipient wetness impregnation method. For this, the required amount of an aqueous solution of a metal salt of a given concentration was added to the CNT support. The description and properties of the CNT support can be found in our previous paper [39]. Cerium nitrate hexahydrate $Ce(NO_3)_3 \cdot 6H_2O$, copper nitrate trihydrate $Cu(NO_3)_2 \cdot 3H_2O$, and ammonium paramolybdate $(NH_4)_6Mo_7O_{24} \cdot 4H_2O$ were used as the precursors of the active component. After the impregnation, MO_x/CNTs samples were dried at 80 °C for 6 h and calcined at 600 °C for 2 h in Ar. The metal content was constant and equal to 20 wt.% of M.

2.2. Characterization of catalysts

The MO_x/CNTs (M = Ce, Mo, Cu) catalysts have been studied by a set of methods: inductively coupled plasma optical emission spectrometry, thermal analysis coupled with mass spectrometry, low-temperature nitrogen adsorption, X-ray diffraction and structural analysis, scanning electron microscopy with EDX analysis and Raman spectroscopy. A description of devices and conditions for studying materials by physicochemical methods can be found in our earlier publications [37, 38, 40].

2.3. Catalytic activity tests

The catalytic activity in the oxidative desulfurization reaction of DBT was measured in a thermostated container quartz reactor. For this, a 25 mg catalyst sample was loaded into the reactor, 20 ml of model fuel was added, heated to 150 °C, and oxygen was supplied at a rate of 15 L/h. A reflux condenser was installed above the outlet of the reactor in order to exclude the entrainment of hydrocarbon fuel components in the gas stream. Model fuel containing 0.5 wt.% DBT or 1000 ppm S was prepared by dissolving DBT in hexadecane ($C_{16}H_{34}$). The reaction time was 6 h. After 6 h, the reactor was cooled, the contents of the reactor were centrifuged to separate the catalyst from the liquid oxidation products, and the total sulfur content in the liquid oxidation products was determined. Further, the liquid oxidation products were divided into two equal parts. One part (after the precipitation of sulfones and sulfoxides due to their low solubility) was analyzed using an Agilent 6890N gas chromatography-mass spectrometer, determining the composition of hydrocarbons in the oxidation products of the model fuel. The second part was mixed with 10 ml of acetonitrile, stirred for 2 h and divided in a separating funnel. In this case, sulfone/sulfoxide

were dissolved in acetonitrile, and unreacted DBT remained in hexadecane. The total sulfur content in the initial fuel and its oxidation products, and the sulfur content as sulfones/sulfoxides dissolved in acetonitrile, was measured using an ASE-2 X-ray energy dispersive sulfur analyzer. The loss of hydrocarbon fuel during the experiment was determined by weighing.

3. Result and discussion

The MO_x/CNTs (M = Ce, Mo, Cu) catalysts were obtained by the incipient wetness impregnation method, in which precursors of the active component are introduced into the pore volume of the support matrix followed by thermal treatment. The characteristics of the decomposition of metal oxide precursors, the evolution of carbon matrix and the formation of catalysts have been studied by thermal analysis (TA) coupled with mass spectrometry (MS). Results of thermogravimetric (TG), differential thermogravimetric (DTG), and differential thermal analysis (DTA) for dried MO_x/CNTs catalysts are presented in Table 1 and Fig. 1. The decomposition of supported Ce, Cu and Mo precursors is a multistage process that includes water desorption, degradation of salt with evolution of NO_x (additionally NH_3 in case of Mo) and degradation of carbon matrix with the evolution of CO_2. Among the studied catalysts, MoO_x/CNT shows the highest temperature of the beginning of CO_2 evolution due to the oxidation/decomposition of CNT support (300 vs. 200 °C). The thermal stability of catalysts improves in the following order of metal Cu < Ce < Mo (Fig. 1).

Table 2 presents the chemical composition, textural and structural characteristics of the MO_x/CNT (M = Ce, Cu, Mo) catalysts after thermal treatment in Ar at 600 °C. Chemical analysis of the samples showed that the metal content corresponds to the calculated amount (20 wt.%), reflecting the successful metal introduction into the carbon matrix.

The specific surface area (S_{BET}) of catalysts depends on the type of M: MoO_x/CNTs shows the lowest S_{BET} of 40 m^2/g, while CuO_x/CNTs exhibits the highest value of 107 m^2/g (Table 2). The pore volume of materials is 0.15–0.18 cm^3/g and increases in the following sequence of metal type Mo < Ce < Cu. According to the data of low-temperature nitrogen adsorption (Fig. 2a), for the CNT support and MO_x/CNT catalysts, adsorption isotherms of type IV with a distinct hysteresis loop of type H3 are observed, which indicates the presence of mesopore structures. Support shows a uniform diameter of 4 nm, while the pore distribution below 6 nm is broadened (Fig. 2b). With the introduction of MO_x, ~ 7 nm pores are additionally observed. Note that S_{BET} of the MO_x/CNTs is lower than the specific surface area of the CNT, which is due to the partial clogging of the pores of the support with MO_x particles [42]. Indeed, the average pore size increases due to a decrease in the proportion of fine

Table 1
TA and MS data for the decomposition of supported Ce, Cu and Mo precursors

Sample*	Weight loss (Δm_i), corresponding to different stages of decomposition (range of ΔT, °C), and total weight loss (Δm_Σ) at 1000 °C, %						DTG peak temperature and type of thermal effect (exo/endo), °C					Evolved gas products in different temperature ranges (ΔT, °C)
	Δm_1	Δm_2	Δm_3	Δm_4	Δm_5	Δm_Σ	T_1	T_2	T_3	T_4	T_5	
CNT	5.6 (500-1000)	-	-	-	-	5.6	500	-	-	-	-	H_2O (25-150) CO_2 (500-1000)
CeO_x/CNT	4.0 (25-130)	6.0 (130-230)	5.0 (230-400)	25.0 (400-1000)	-	40.0	80 endo	170	215	-	-	H_2O (25-400) NO_x (100-400) CO_2 (230-1000)
CuO_x/CNT	2.0 (25-200)	8.8 (200-320)	6.9 (220-600)	7.7 (625-1000)	-	25.4	245 endo	570 endo	-	-	-	H_2O (25-400) NO_x (200-1000) CO_2 (200-1000)
MoO_x/CNT	1.3 (25-140)	1.4 (140-400)	11.8 (400-1000)	-	-	14.5	70	200	680 endo	-	-	H_2O (25-500) NH_3 (25-500) NO (230-500) NO_2 (300-1000) CO_2 (300-1000)

* M content is equal to 10 wt.%

(a)

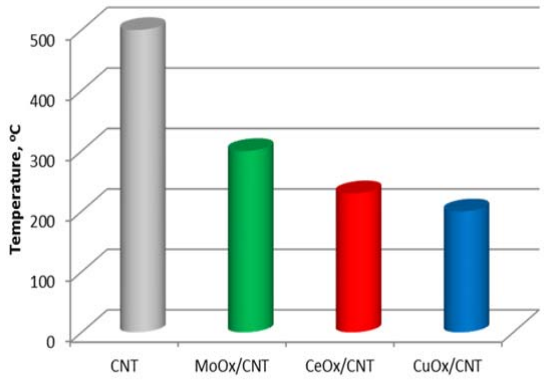

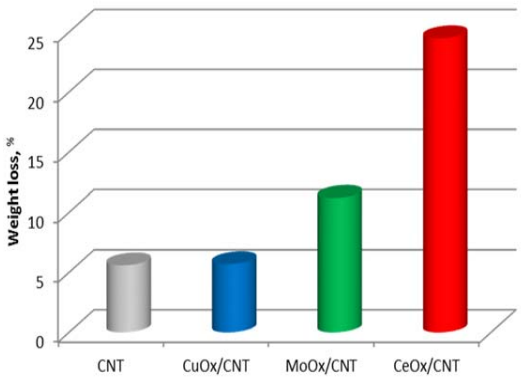

(b)

Fig. 1. The temperature of the beginning of CO_2 evolution (a) and weight loss (b) due to the oxidation/decomposition of CNT support during the thermal treatment of the dried MO_x/CNT (M = Ce, Cu, Mo) catalysts. M content is equal to 10 wt.%.

pores. This is manifested to a greater extent for the MoO_x/CNTs catalyst, the average pore diameter of which is doubled in comparison with the support (Table 2). Pores with a size of 7–20 nm are considered optimal for removing DBT and its alkyl-substituted derivatives by the HDS [43, 44].

The X-ray diffraction patterns of the support show the diffraction peaks at 2Θ: 25–26°, 42° and 54°, which were attributed to the (002), (101), and (004) crystal planes of hexagonal graphite (JCPDS no. 41-1487). The major diffraction peaks for nickel Ni (44.4°, 51.8° and 76.3°) and mixed nickel-magnesium oxide NiO-MgO (37.1°, 43.2° and 62.6°) phases are also observed, which is connected with the preparation mode of CNTs. The incorporation of metal had no practically effect on the structure of the carbon support (Fig. 3). For MO_x/CNTs samples, the emergence of new diffraction peaks was attributed to CeO_2 (28.5°, 33.0°, 47.5° and 56.3°) in the case of CeO_x/CNTs; Cu° (43.2°, 50.3°, 73.9°), Cu_2O (36.2°, 42.2°) and CuO (35.5°, 38.8°, 51.5, 75.8°) in the case of CuO_x/CNTs; and MoO_2 (37.1°, 54.2°) and MoO_3 (23.4, 27.4, 33.1) in the case of MoO_x/CNTs. Despite the high content of the active component, rather high dispersion of oxide particles is observed: 12–13 nm in size for M = Ce and Mo; 25–28 nm in size for M = Cu (Table 2). The formation of Cu, Cu_2O and MoO_2

Table 2

Chemical composition, textural and structural characteristics of the MO_x/CNT (M = Ce, Cu, Mo) catalysts

Sample	Content, wt. %	Textural characteristics			XRD data*			Raman spectroscopy data, I_D/I_G
		S_{BET}, m^2/g	V_p, cm^3/g	D_p, nm	Phase composition	Cell parameter, Å	CSR**, nm	
CNT	-	180	0.33	7.5	C (hex.) MgO-NiO Ni	c = 6.810 a = 4.195 a = 3.529	6.0 21.0 30.0	1.93
CeO_x/CNT	19.9±0.2	101	0.18	7.2	C (hex.) MgO-NiO Ni CeO_2	c = 6.811 - a = 3.521 a = 5.404	- - 20.0 12.0	1.47
CuO_x/CNT	20.1±0.1	107	0.23	8.5	C (hex.) CuO Cu_2O Cu	c = 6.811 - a = 4.264 a = 3.609	6.0 - 25.0 28.0	1.58
MoO_x/CNT	19.2±0.1	40	0.15	14.3	C (hex.) MoO_2 MoO_3	- a = 4.828 -	- 13.0 -	1.30

* a dash in the XRD data means that the determination of structural parameters is difficult due to the superposition of reflections and a low phase content; ** coherent scattering region.

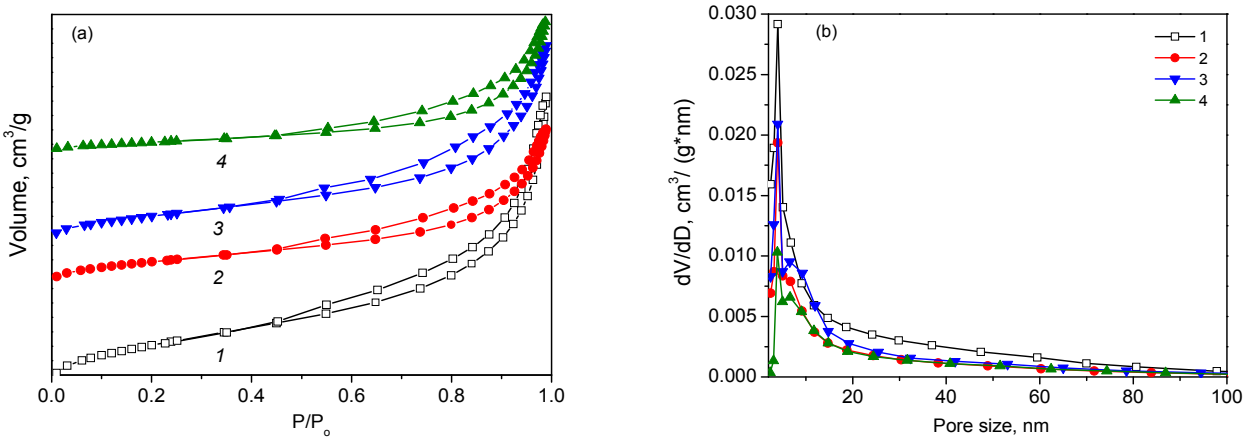

Fig. 2. N_2 adsorption-desorption isotherms (a) and pore size distributions (b) for MO_x/CNTs catalysts: 1 – CNTs; 2 – CeO_x/CNT; 3 – CuO_x/CNT; 4 – MoO_x/CNT.

phases indicates that the decomposition of the carbon supported precursor is accompanied by the partial reduction of the cations of the active component. Similar results were demonstrated in [42, 45–47]. An increase in the calcination temperature in an inert atmosphere or the use of a reducing medium during calcination leads to the formation of molybdenum carbide [46]. The strong interaction of metal oxides with CNTs facilitates their auto-reduction during the thermal treatment in inert media. It was shown that metal-support interaction growth with the decrease of the inner diameter of CNTs is favorable for the entry of metal species into the cavity and their stabilization in a highly dispersed state [42]. Our CNTs are multi-walled nanotubes with an inner diameter of 10–20 nm. So, for the MO_x/CNTs, the moderate metal-support interaction is realized, providing the formation of the partly reduced metal oxides particles, the size of which is comparable to the inner diameter of CNTs.

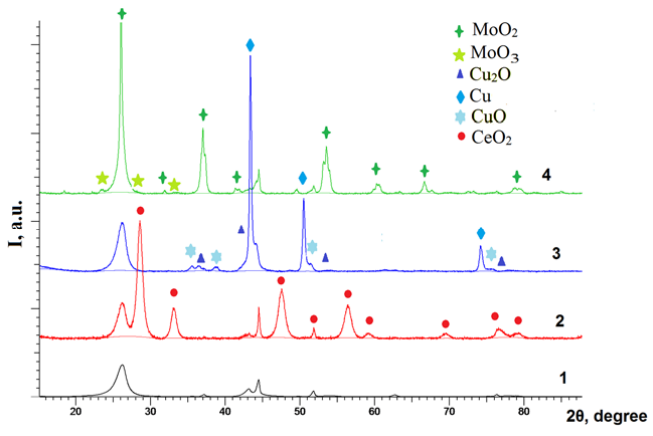

Fig. 3. XRD patterns of MO_x/CNTs catalysts: 1 – CNT; 2 – CeO_x/CNT; 3 – CuO_x/CNT; 4 – MoO_x/CNTs.

X-ray phase analysis data are in good correlation with the results of Raman spectroscopy (Fig. 4). For the CeO_x/CNTs sample, the band with a maximum at 462 cm^{-1} was registered attributed to CeO_2, which has a cubic crystal structure of the fluorite type. The Raman spectrum of cerium (IV) oxide exhibits only one allowed Raman mode, 465 cm^{-1} F_{2g} [48]. The band's shift to a shorter wavelength region may mean that the oxide phase has defects, most likely due to the size effect. The Raman spectrum of CuO_x/CNTs is notable for the presence of rather narrow bands at 150 cm^{-1} and 220 cm^{-1} and a wide band centered at 640 cm^{-1}. These bands are characteristic of Cu_2O [49]. For the MoO_x/CNTs catalyst, bands with maximum intensity at 128, 205, 230, 349, 365, 425, 498, 572 and 743 cm^{-1} can be clearly distinguished (Fig. 4c). A similar set of bands (with slight changes in positions) is characteristic of monoclinic MoO_2 [50].

In the spectral range of the Raman shift of 900–1900 cm^{-1} the studied samples had two Raman-active bands at about 1580 (G band) and 1340 cm^{-1} (D band), the intensity ratio of which (I_D/I_G) is the indication of the orderliness of the graphite structure [51]. So, the defectiveness of CNTs for studied materials was estimated by the value I_D/I_G (Table 2, Fig. 4d). For unmodified CNTs, this parameter is equal to 1.93, while for MO_x/CNTs, it is slightly lower, which indicates the decrease of the content of amorphous carbon, as well as a decrease in the number of defects [52]. In particular, the disordering of the carbon matrix of support increases in the following row of M: Mo < Ce < Cu. Note that it is accomplished by a growth of the specific surface area and a decrease of metal oxides dispersion.

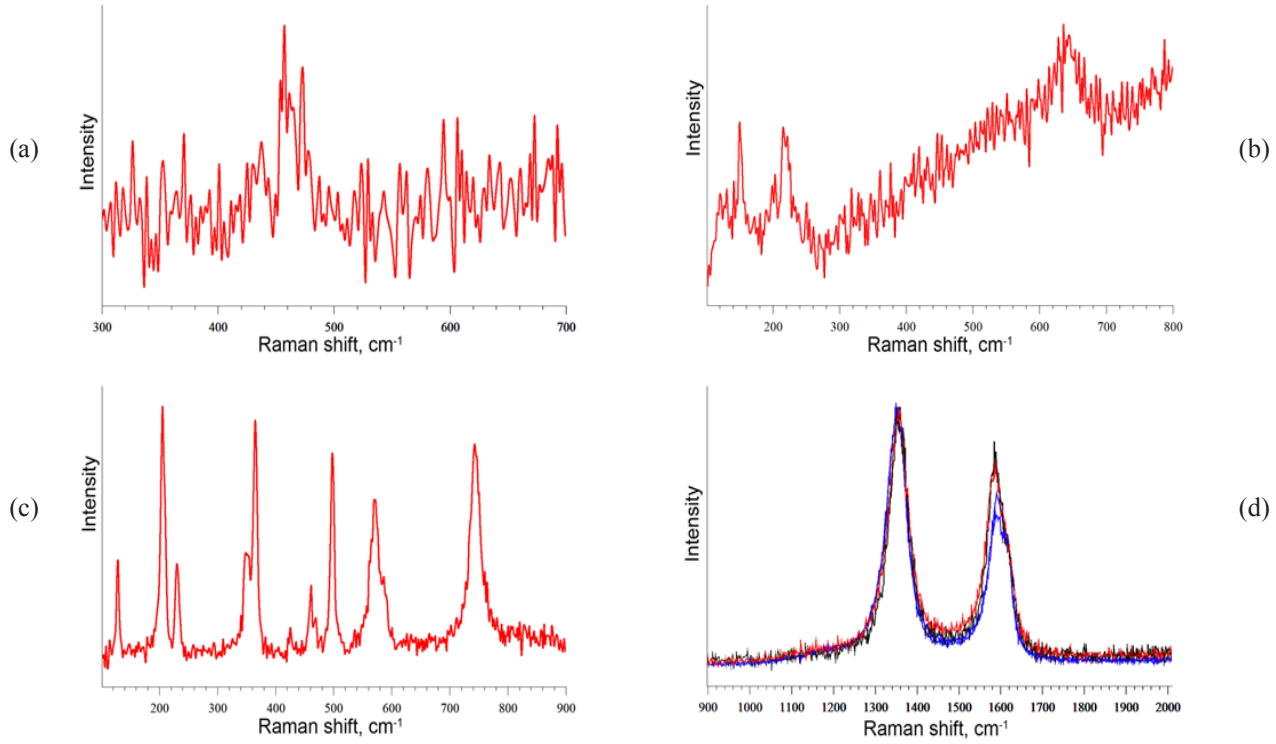

Fig. 4. Raman spectra of samples: CeO_x/CNT (a), CuO_x/CNT (b) and MoO_x/CNT (4) in the spectral range of the Raman shift of 100 ÷ 900 cm^{-1} (a-c) and 900 ÷ 1900 cm^{-1} (d).

The energy-dispersive X-ray spectroscopy confirmed the homogenous distribution of M throughout the CNT support (Fig. 5). The molar ratio O/C for CNTs is equal to 0.1 and does not change after supporting metal oxides.

Oxidation of DBT proceeds along two routes, the common intermediate products of which are DBT sulfoxide and sulfone (Scheme 1) [10,18]. The product of selective elimination of SO_2 is diphenyl, and the products of deep oxidation are

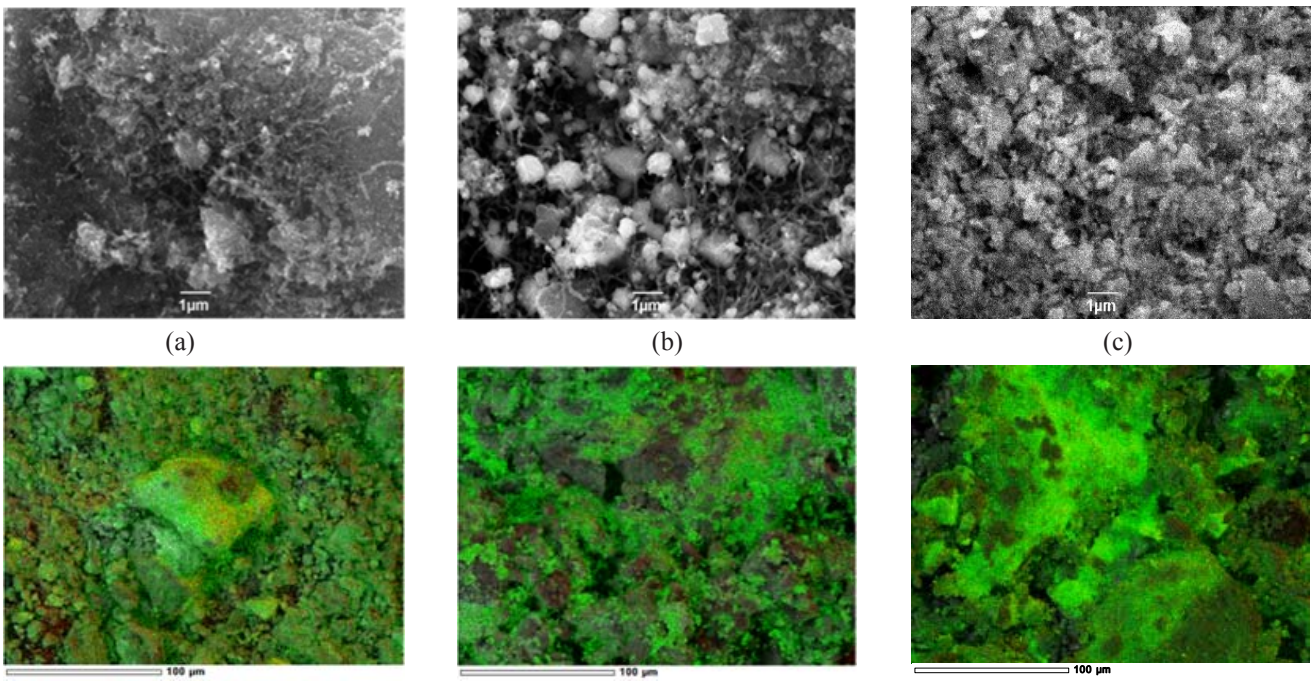

Fig. 5. SEM images of samples CeO_x/CNT (a, d), CuO_x/CNT (b, e), MoO_x/CNT (c, f), obtained in the registration mode of reflected electrons (a, b, c) and characteristic X-ray radiation O (red), M (green) images (d, e, f) – with superposition of all signals.

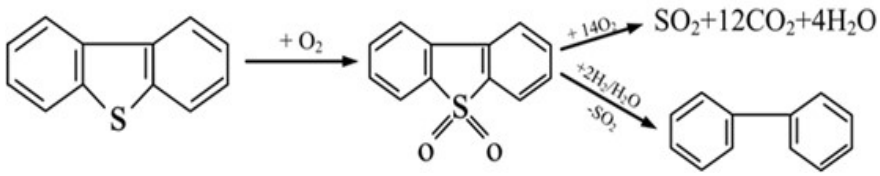

Scheme 1. Oxidative transformation of DBT.

SO_2, CO_2 and H_2O. DBT and its sulfone can often be retained on the catalyst surface, up to the formation of sulfide and sulfate phases of the active component due to the formation of strong bonds with functional groups of the support surface and active centers of transition metal oxides [10, 11]. Chemisorption of the sulfur compound and its sulfone on the catalyst surface further contributes to the overall removal of the sulfur compound from hydrocarbon fuels. The contribution of chemisorption depends on the concentration and nature of the active component, which determines the sorption capacity of the catalyst [18]. The contribution of chemisorption is apparently more significant in batch reactors than in flow reactors.

Figure 6 illustrates the catalytic performance: the total conversion of DBT and the conversion of DBT to DBT-SO_2, achieved on catalysts for 6 h at a temperature of 150 °C. The maximum total conversion of DBT, reaching 95–99% values, is demonstrated by the MoO_x/CNTs sample, the minimum (about 67%) by the CeO_x/CNTs sample. However, the conversion of DTB to sulfone on all catalysts was significantly lower than the total conversion of DBT. The conversion of DBT to sulfone increased in the series of metals: Mo < Ce < Cu from 44 to 51%. The observed differences in the total conversion of DBT and in the formation of sulfone (DBT-to-$DBTSO_2$) can be explained by two reasons. First, the SO_2 can be formed and removed from the reactor together with the gas reaction products. However, during the first 1–3 h of the experiment, we were unable to detect SO_2 in the gas reaction products using gas chromatographic analysis. Secondly, DBT and/or sulfone can be adsorbed on the catalyst surface. The differences between the total conversion of DBT and the formation of sulfone change in the series Ce < Cu < Mo, which correlates with the tendency of catalyst elements to sulfidation.

It should be noted that the maximum conversions of the hydrocarbon part of the fuel ($C_{16}H_{34}$) are observed in the presence of the CuO_x/CNTs catalyst. The mass of liquid oxidation products of the model fuel obtained in the presence of CuO_x/CNTs

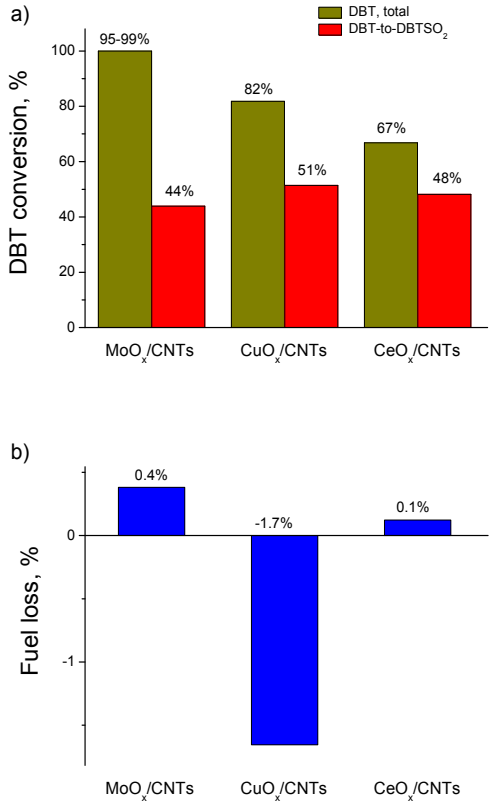

Fig. 6. DBT conversion (a) and fuel loss (b) over MO_x/CNTs catalysts in aerobic oxidative desulfurization of a model diesel fuel. Reaction conditions: 99.5% $C_{16}O_{34}$, 0.5% DBT, 150 °C, duration 6 h.

increased during the experiment by 1.7%, and the fuel itself was colored, probably due to the formation of oxygenates. In the case of MoO_x/CNTs and CeO_x/CNTs, the loss of hydrocarbon fuel did not exceed 0.4%, and the oxidation products remained transparent and colorless. The observed trend correlates with the fact that CuO_x is part of the catalysts for the oxidation of heavy hydrocarbons, providing their high conversion in deep oxidation reactions [53].

4. Conclusions

CNT-supported MO_x catalysts with different metal types (M = Ce, Cu, Mo) were prepared and

used for aerobic oxidative desulfurization of a model diesel fuel. A complex of physicochemical methods (inductively coupled plasma optical emission spectrometry, thermal analysis coupled with mass spectrometry, low-temperature nitrogen adsorption, X-ray diffraction and structural analysis, scanning electron microscopy with EDX analysis, Raman spectroscopy) established the patterns of the formation of samples and their main properties. The samples are characterized by a developed mesoporous structure and a dispersed state of the active component. The crystals observed in their composition were CeO_2, $CuO/Cu_2O/Cu$, or MoO_3/MoO_2. The functional properties of the catalysts is controlled by types of the active component (M = Ce, Cu, Mo). The total conversion of dibenzothiophene at 150 °C increased in the following row of M: Ce < Cu < Mo. The MoO_x/CNTs catalysts are most promising for innovative technology for the purification of motor fuel to the EURO-5 standard by oxidative desulfurization. It provides 95–99% dibenzothiophene conversion, which is associated with both the oxidizing ability and the tendency of MoO_x to chemisorption of sulfur compounds.

Acknowledgments

This study was financially supported by the Russian Science Foundation (Project No. 19-13-00129). This study was accomplished using the research facilities of the FRC CCC of SB RAS.

References

[1]. Cleaning up the global on-road diesel fleet, (2016). https://wedocs.unep.org/bitstream/handle/20.500.11822/21552/Cleaning_up_Global_diesel_fleet.pdf?sequence=1&amp%3BisAllowed=

[2]. B. Zhang. Chapter 1: Hydroprocessing and the Chemistry. Hydroprocessing Catalysts and Processes, 2018, pp. 1–56. DOI: 10.1142/9781786344847_0001

[3]. Z. Chen, L. Ling, B. Wang, H. Fan, J. Shangguan, J. Mi, *Appl. Surf. Sci.* 387 (2016) 483–490. DOI: 10.1016/j.apsusc.2016.06.078

[4]. H. Zhu, X. Li, N. Shi, X. Ding, Z. Yu, W. Zhao, H. Ren, Y. Pan, Y. Liu, W. Guo, *Catal. Sci. Technol.* 11 (2021) 1615–1625. DOI: 10.1039/d0cy01523g

[5]. P. Wu, W. Zhu, B. Dai, Y. Chao, C. Li, H. Li, M. Zhang, W. Jiang, H. Li, *Chem. Eng. J.* 301 (2016) 123–131. DOI: 10.1016/j.cej.2016.04.103

[6]. N. Lv, L. Sun, L. Chen, Y. Li, J. Zhang, P. Wu, H. Li, W. Zhu, H. Li, *Phys. Chem. Chem. Phys*. 21 (2019) 21867–21874. DOI: 10.1039/c9cp03758f

[7]. L. Dai, Y. Wei, X. Xu, P. Wu, M. Zhang, C. Wang, H. Li, Q. Zhang, H. Li, W. Zhu, *ChemCatChem* 12 (2020) 1734–1742. DOI: 10.1002/cctc.201902088

[8]. J. Xiao, L. Wu, Y. Wu, B. Liu, L. Dai, Z. Li, Q. Xia, H. Xi, *Appl. Energ.* 113 (2014) 78–85. DOI: 10.1016/j.apenergy.2013.06.047

[9]. S.A. Yashnik, M.A. Kerzhentsev, A.V. Salnikov, Z.R. Ismagilov, A. Bourane, O.R. Koseoglu, *Kinet. Catal.* 56 (2015) 466–475. DOI: 10.1134/S0023158415040205

[10]. S.A. Yashnik, A.V. Salnikov, M.A. Kerzhentsev, A.A. Saraev, V.V. Kaichev, L.M. Khitsova, Z.R. Ismagilov, J. Yamin, O.R. Koseoglu, *Kinet. Catal.* 58 (2017) 58–72. DOI: 10.1134/S0023158417010128

[11]. Z.R. Ismagilov, M.A. Kerzhentsev, S.A. Yashnik, S.R. Khairulin, A. V. Salnikov, V.N. Parmon, A. Bourane, O.R. Koseoglu, *Eurasian Chem.-Technol. J.* 17 (2015) 119–128. DOI: 10.18321/ectj202

[12]. H. Mohumed, S. Rahman, S.A. Imtiaz, Y. Zhang, *ACS Omega* 5 (2020) 8023–8031. DOI: 10.1021/acsomega.0c00096

[13]. X. Zeng, X. Xiao, Y. Li, J. Chen, H. Wang, *Appl. Catal. B Environ*. 209 (2017) 98–109. DOI: 10.1016/j.apcatb.2017.02.077

[14]. I. Shafiq, S. Shafique, P. Akhter, M. Ishaq, W. Yang, M. Hussain, *J. Clean. Prod.* 294 (2021) 125731. DOI: 10.1016/j.jclepro.2020.125731

[15]. A. Rajendran, T.Y. Cui, H.X. Fan, Z.F. Yang, J. Feng, W.Y. Li, *J. Mater. Chem. A.* 8 (2020) 2246–2285. DOI: 10.1039/c9ta12555h

[16]. K.M. Dooley, D. Liu, A.M. Madrid, F.C. Knopf, *Appl. Catal. A Gen.* 468 (2013) 143–149. DOI: 10.1016/j.apcata.2013.08.013

[17]. E.A. Eseva, A.V. Akopyan, A.V. Anisimov, A.L. Maksimov, *Pet. Chem.* 60 (2020) 979–990. DOI: 10.1134/S0965544120090091

[18]. Z. Ismagilov, S. Yashnik, M. Kerzhentsev, V. Parmon, A. Bourane, F.M. Al-Shahrani, A.A. Hajji, O.R. Koseoglu, *Catal. Rev.* 53 (2011) 199–255. DOI: 10.1080/01614940.2011.596426

[19]. X. Bin Lim, W.-J. Ong, *Nanoscale Horizons.* 6 (2021) 588–633. DOI: 10.1039/d1nh00127b

[20]. J.T. Sampanthar, H. Xiao, J. Dou, T.Y. Nah, X. Rong, W.P. Kwan, *Appl. Catal. B Environ.* 63 (2006) 85–93. DOI: 10.1016/j.apcatb.2005.09.007

[21]. Y. Lu, Y. Wang, L. Gao, J. Chen, J. Mao, Q. Xue, Y. Liu, H. Wu, G. Gao, M. He, *ChemSusChem* 1 (2008) 302–306. DOI: 10.1002/cssc.200700144

[22]. X. Ma, A. Zhou, C. Song, *Catal. Today.* 123 (2007) 276–284. DOI: 10.1016/j.cattod.2007.02.036

[23]. Q. Zhang, J. Zhang, H. Yang, Y. Dong, Y. Liu, L. Yang, D. Wei, W. Wang, L. Bai, H. Chen, *Catal. Sci. Technol.* 9 (2019) 2915–2922. DOI: 10.1039/c9cy00459a
[24]. C. Wang, Z. Chen, X. Yao, W. Jiang, M. Zhang, H. Li, H. Liu, W. Zhu, H. Li, *RSC Adv.* 7 (2017) 39383–39390. DOI: 10.1039/c7ra07286d
[25]. Y. Shi, G. Liu, B. Zhang, X. Zhang, *Green Chem.* 18 (2016) 5273–5279. DOI: 10.1039/c6gc01357k
[26]. F.L. Yu, C.Y. Liu, B. Yuan, C.X. Xie, S.T. Yu, *Catal. Commun.* 68 (2015) 49–52. DOI: 10.1016/j.catcom.2015.04.029
[27]. M. Zhang, W. Liao, Y. Wei, C. Wang, Y. Fu, Y. Gao, L. Zhu, W. Zhu, H. Li, *ACS Appl. Nano Mater.* 4 (2021) 1085–1093. DOI: 10.1021/acsanm.0c02639
[28]. M. Shi, D. Zhang, X. Yu, Y. Li, X. Wang, W. Yang, *Fuel Process. Technol*. 160 (2017) 136–142. DOI: 10.1016/j.fuproc.2017.02.038
[29]. Q. Gu, G. Wen, Y. Ding, K.H. Wu, C. Chen, D. Su, *Green Chem.* 19 (2017) 1175–1181. DOI: 10.1039/c6gc02894b
[30]. W. Zhang, H. Zhang, J. Xiao, Z. Zhao, M. Yu, Z. Li, *Green Chem.* 16 (2014) 211–220. DOI: 10.1039/c3gc41106k
[31]. Q. Gu, Y. Lin, S. Heumann, D. Su, *Chem. - Asian J.* 12 (2017) 2876–2883. DOI: 10.1002/asia.201700995
[32]. Y. Gao, Z. Lv, R. Gao, G. Zhang, Y. Zheng, J. Zhao, *J. Hazard. Mater.* 359 (2018) 258–265. DOI: 10.1016/j.jhazmat.2018.07.008
[33]. O.Y. Podyacheva, A.N. Suboch, S.A. Yashnik, A.V. Salnikov, S.V. Cherepanova, L.S. Kibis, G.Y. Simenyuk, A.I. Romanenko, Z.R. Ismagilov, *J. Struct. Chem.* 62 (2021) 771–781. DOI: 10.1134/S0022476621050139
[34]. E. Pérez-Mayoral, V. Calvino-Casilda, E. Soriano, *Catal. Sci. Technol.* 6 (2016) 1265–1291. DOI: 10.1039/c5cy01437a
[35]. B.N. Bhadra, N.A. Khan, S.H. Jhung, *J. Mater. Chem. A*. 7 (2019) 17823–17833. DOI: 10.1039/c9ta03613j
[36]. J. Chen, X. Wang, D. Wu, J. Zhang, Q. Ma, X. Gao, X. Lai, H. Xia, S. Fan, T.S. Zhao, *Fuel* 239 (2019) 44–52. DOI: 10.1016/j.fuel.2018.10.148
[37]. Z.R. Ismagilov, E.V. Matus, O.S. Efimova, L.M. Khitsova, A.N. Popova, A.P. Nikitin, S.A. Sozinov, *Eurasian Chem-Techol. J.* 22 (2020) 81–88. DOI: 10.18321/ectj954
[38]. E.V. Matus, O.S. Efimova, A.N. Popova, A.P. Nikitin, S.A. Sozinov, Z.R. Ismagilov, *J. Phys. Conf. Ser.* 1749 (2021). DOI: 10.1088/1742-6596/1749/1/012022
[39]. Z.R. Ismagilov, S.A. Yashnik, N.V. Shikina, E.V. Matus, O.S. Efimova, A.N. Popova, A.P. Nikitin, *Eurasian Chem.-Techol. J.* 21 (2019) 291–302. DOI: 10.18321/ectj886
[40]. E.V. Matus, L.M. Khitsova, O.S. Efimova, S.A. Yashnik, N.V. Shikina, Z.R. Ismagilov, *Eurasian Chem.-Techol. J.* 21 (2019) 303–316. DOI: 10.18321/ectj887
[41]. L.B. Okhlopkova, O.S. Efimova, L.M. Khitsova, Z.R. Ismagilov, *Chem. Sustain. Dev.* 28 (2020) 566–575. DOI: 10.15372/CSD2020266
[42]. D. Zhao, G. Zhang, L. Yan, L. Kong, H. Zheng, J. Mi, Z. Li, *Catal. Sci. Technol.* 10 (2020) 2615–2626. DOI: 10.1039/c9cy02407g
[43]. M.V.C. Sekhar, *Stud. Surf. Sci. Catal.* 38 (1988) 383–392. DOI: 10.1016/S0167-2991(09)60671-6
[44]. Y. Okamoto, *Bull. Chem. Soc. Jpn.* 87 (2014) 20–58. DOI: 10.1246/bcsj.20130204
[45]. H. Shang, C. Liu, Y. Xu, J. Qiu, F. Wei, *Fuel Process. Technol.* 88 (2007) 117–123. DOI: 10.1016/j.fuproc.2004.08.010
[46]. M. Güler, D. Varişli, *Turkish J. Chem.* 44 (2020) 309–324. DOI: 10.3906/KIM-1907-4
[47]. D. Deng, N. Chen, Y. Li, X. Xing, X. Liu, X. Xiao, Y. Wang, *Physica E* 86 (2017) 284–291. DOI: 10.1016/j.physe.2016.10.031
[48]. B.M. Reddy, A. Khan, Y. Yamada, T. Kobayashi, S. Loridant, J.C. Volta, *J. Phys. Chem. B*. 107 (2003) 11475–11484. DOI: 10.1021/jp0358376
[49]. Y. Deng, A.D. Handoko, Y. Du, S. Xi, B.S. Yeo, *ACS Catal.* 6 (2016) 2473–2481. DOI: 10.1021/acscatal.6b00205
[50]. M. Dieterle, G. Mestl, *Phys. Chem. Chem. Phys.* 4 (2002) 822–826. DOI: 10.1039/b107046k
[51]. V. Gupta, T.A. Saleh, Composites; Adsorption and Photo-degradation. Carbon Nanotubes - From Research to Applications (2011). DOI: 10.5772/18009
[52]. R.A. DiLeo, B.J. Landi, R.P. Raffaelle, *J. Appl. Phys.* 101 (2007) 064307. DOI: 10.1063/1.2712152
[53]. I. Heo, M.H. Wiebenga, J.R. Gaudet, I.S. Nam, W. Li, C.H. Kim, *Appl. Catal. B Environ.* 160–161 (2014) 365–373. DOI: 10.1016/j.apcatb.2014.05.045